PCCP

PAPER

View Article Online
View Journal

Cite this: DOI: 10.1039/c5cp00115c

Ab initio and anion photoelectron study of Au_nRh_m (n = 1–7, m = 1–2) clusters†

Fernando Buendía,[a] Marcela R. Beltrán,*[a] Xinxing Zhang,[b] Gaoxiang Liu,[b] Allyson Buytendyk[b] and Kit Bowen[b]

Received 8th January 2015,
Accepted 13th March 2015

DOI: 10.1039/c5cp00115c

www.rsc.org/pccp

Anion photoelectron spectroscopy (PES) and *ab initio* calculations have been used to identify the unique structural, electronic, and magnetic properties of both neutral and anionic binary Au_nRh_m (n = 1–7 and m = 1–2) clusters *in vacuo*. Negative ion photoelectron spectra are presented with electron binding energies measured up to 3.493 eV. We discuss our computational results in the context of the PES experiment, in which the calculated electron affinities and vertical detachment energies are in good agreement with the measured values. Theoretically, we investigate the low-lying energy structures and the spin isomers of each neutral, anionic and cationic species. The PES spectra, binding energies, fragmentation energy, electron affinities, vertical and adiabatic detached energies, HOMO–LUMO (H–L) gaps and vibrational spectra are presented and discussed. Our results show that the characteristic planarity for gold clusters is preserved for many of the bimetallic clusters. This study is therefore compared with the case of pure gold for which ample experimental and theoretical data are available. Both experimental and theoretical results obtained here are compared and discussed with previous theoretical studies on the same systems.

1 Introduction

A detailed knowledge of the geometry and the electronic structures of atomic clusters is necessary to understand the evolution of their properties with size toward the macroscopic scale. This aspect is particularly important for systems wherein novel non-bulk like properties emerge at the nano-scale. For example, one such novel phenomenun is the peculiar catalytic behavior of gold at selective size clusters.[1] Moreover, rhodium, which is well known as a heterogeneous catalyst, exhibits a striking magnetic behavior at the nanoscale.[2–6] Additionally, there are many cases where adding a second metal enhances the catalytic properties. In light of these observations we undertook a systematic study of bimetallic Au_nRh_m clusters. The study has been performed for Au_nRh_m cluster sizes with n = 1–7, m = 1–2 atoms. Our aim is to unveil their geometric structures as well as their electronic signatures in order to study O_2 and CO adsorption on their surfaces in a future study. With this eventual goal in mind, it is of paramount importance that we fully characterize the isolated (*in vacuo*) clusters. For this reason, we utilized the combination of photo electron spectroscopy (PES) on the anionic clusters and calculations based on density functional theory (DFT). We based our research on recent developments in the area of nano clusters, and the size dependence of their catalytic properties, the latter of which can be achieved by either size-selecting clusters prior to deposition on well characterized surfaces or by investigating individual clusters in the gas phase.[7] The study of gold clusters is amongst the most active topic in nano science both, from the experimental as well as the theoretical point of view. Nevertheless, the nano alloys formed with gold have been less explored, especially those with late transition elements such as rhodium, where research is needed to reveal their properties, there being only few such studies found in the literature.[8,9] For gold, most experimental work is related to determining its geometric structure and has been performed on charged clusters due to the ease of mass separation and thereby size-selection. These studies give insight into a structural evolution that is completely different from other metals. The most characteristic aspect being its transition from 2- to 3-dimensional structures[10,11] in cluster sizes $\geq$12 depending on the charged state. For example, a recent study based on a combined FIR-MPD and *ab initio* calculations confirms planar structures for up to 8 atom clusters.[12] Au_{19} and Au_{20} have been also experimentally confirmed and are non-planar.[13,14] For the cationic ones, the smallest cluster with a non-planar geometry is Au_8, while for the anions the

[a] Instituto de Investigaciones en Materiales, Universidad Nacional Autónoma de México, Circ. ext. s/n Apdo. Postal 70-360, C.P. 04510, México D.F., Mexico. E-mail: mbeltran@unam.mx; Tel: +52 55 5622 4624

[b] Department of Chemistry, Johns Hopkins University, Baltimore, MD 21218, USA

† Electronic supplementary information (ESI) available: Cartesian coordinates for all neutral cation and anionic clusters, a list of coordinates for high energy isomers, and figures for cationic lowest energy structures. See DOI: 10.1039/c5cp00115c

crossover between planar and non-planar structures is found around the 12-atoms with co-existing planar and non-planar structures. By performing experiments on gold in the gas phase their ionization potentials have been determined by threshold electron impact ionization.[15] From the theory point of view the small sized planar structures have been well studied in ref. 1 and 16–25. From all these studies, it has been found that both their transition sizes as well as the predicted ground state structures depend on the theoretical methods used and how relativistic effects and dispersion interaction are considered. In the case of rhodium clusters, studies have been performed to establish their role in catalysis in this size regime.[26–33] Recent photo electron spectroscopy (PES) studies combined with theory as well as joint far-infrared multiple photon dissociation (FIR-MPD) experiments supported by DFT studies on Rh_n clusters elucidated their geometries for all the neutral as well as for charged states between n = 2–9 cluster sizes.[2,32,33] Additionally, the reactivity of CO on Rh_n clusters has been studied in.[26–31] Those studies showed the importance of the precise determination of the geometric structures of transition metal clusters. Another interesting aspect of rhodium concerns its magnetic properties. Experiments show that small rhodium clusters with less than 60 atoms have non-zero magnetic moments.[34,35] Theoretically many studies have been performed to determine their electronic structures.[2–5] The present considers the study of the electronic and vibrational properties of anions, cations and neutral clusters. The experimental negative ion photo electron spectra are discussed in terms of the theoretical predictions by comparing the calculated electron affinities and vertical detachment energies with the measured values. Their predicted infrared spectra, their magnetic moment, the defragmentation energy and their H–L gaps are discussed. For these purposes, we have explored theoretically not only the lowest energy structures and their spin manifold in all cases (neutral and charged clusters) but also a number of higher energy isomers in order to corroborate the experimental findings.

2 Experiment

Negative ion photoelectron spectroscopy is conducted by crossing a beam of mass selected anions with a fixed-frequency photon beam and energy analyzing the resultant photodetached electrons. The photodetachment process is governed by the energy conserving relationship, $h\nu$ = EBE + EKE, where $h\nu$ is the photon energy, EBE is the electron binding energy, and EKE is the electron kinetic energy. Our apparatus has been described previously elsewhere.[36,37] Briefly, the apparatus consists of an ion source, a linear time-of-flight (TOF) mass spectrometer, a photodetachment laser, and a magnetic bottle photoelectron spectrometer (MB-PES). The instrumental resolution of the MB-PES is ~35 meV at 1 eV EKE. The third harmonic (355 nm, 3.493 eV) of a Nd:YAG laser was used to photodetach the cluster anions of interest. Photoelectron spectra were calibrated as in ref. 36 and 37 against the well known atomic transitions of Cu^-. In the current study, rhodium gold cluster anions were generated in a laser vaporization disk source. A rhodium gold disk was prepared by pressing the mixed powder at a pressure of ~170 MPa. The disk was ablated by a pulsed Nd:YAG laser beam of 532 nm photons. The plasma was cooled by supersonically expanding a plume of helium carrier gas issued from a general pulsed valve with a backing pressure of ~1 MPa. The negatively charged clusters were then extracted into our spectrometer for photoelectron spectroscopy studies.

3 Theory

The theoretical part of this study has been performed under the framework of the density functional theory (DFT) approximation. The TURBOMOLE V6.4 package has been used.[38] The RI-J method was employed for speeding reasons as it saves time on calculating the Coulomb integrals at each step. We have employed the def2-TZVP basis set (with the associated effective core potential def2-ecp)[39]and the exchange and correlation functional proposed by Perdew, Becke and Ernzerhof.[40] The suitability of such type of functionals for the investigation of gold clusters has been widely used in the past and has been discussed previously.[41,42] The convergence parameter for the energy in the self-consistent field is 10^{-6} Ha. While the conjugated gradient forces were converged to 10^{-3} Ha $Bohr^{-1}$, the Hartree energy is converged to 10^{-6} Ha at each cycle. The calculation has been performed under the internal coordinates framework, and no symmetry restrictions have been imposed during the minimization process. Once the structures were properly converged a tolerance of 0.1 Å has been used to elucidate the cluster group symmetry. With this theoretical framework we have produced Table 1, which shows our calculated values for the Au–Au, Rh–Rh and Au–Rh dimer distances and frequencies. The calculated harmonic vibrational frequencies were obtained initially as a viable tool to verify true low energy landscape minima states and also because this quantity can be compared directly with future experimental (FIR-MPD) spectra on the same systems. The IR spectra are calculated only for the lowest-energy isomers. To calibrate our methodology, we compared calculated IR with experimental FIR-MPD on small gold clusters (4–7 atoms),[12] and our IR spectra agree very well. We identify the participating species in the experimental PES through the quantitative agreement between the calculated (VDE), from the anion ground state with multiplicity M to neutral species (at the anion geometry) with multiplicity $M \pm 1$, with the experimental peaks. To extract this result, we do consider that the ionic cluster has an N number of unpaired spins and therefore a magnetic moment of $N\mu_B$ and a spin multiplicity of

Table 1 Comparison between the available experimental and theoretical data with the present work

	ω_e (cm^{-1})			r_e (Å)			E_b (eV)		
	Exp.	Theo.[a]	Res.	Exp.	Theo.[a]	Res.	Exp.	Theo.[a]	Res.
Au_2	191[b]	170	171	2.47[b]	2.54	2.53	2.29[b]	2.30	2.23
Rh_2	267[c]	289	283	2.28[c]	2.32	2.29	—	2.90	2.67
AuRh	—	199	196	—	2.52	2.50	—	2.64	2.41

[a] For previous theoretical values see ref. 8. [b] For previous experimental values see ref. 43. [c] For previous experimental values see ref. 44.

$M = N + 1$. [The spin magnetic moment is related with the multiplicity as follows $2S + 1 = M$.] As an electron is detached, the neutral cluster can have a multiplicity of $M + 1$ or $M - 1$, depending upon whether the electron was removed from the minority or majority state. Nevertheless theoretical interpretation of the PES spectra is not necessarily straightforward. As the cluster size increases, more issues need to be taken into consideration when calculating these energies for them to match the experimental data. The ground state structures of the anion and its corresponding neutral are not necessarily the same, in fact they can be quite different. When this occurs it leads to a broad peak in the experimental spectrum. This complicates the interpretation of the PES peak assignments. Another issue to be considered is the presence of several low lying structural isomers and spin multiplicities close in energy at each cluster size. Therefore, the calculations were performed for a number of possible structures for both charged and neutral Au_nRh_m clusters (for n = 1–7, m = 1–2). We explored all inequivalent positions for the Au and Rh atoms as well. The lowest energy isomers together with their spin multiplicity symmetry group and electronic state are shown in Fig. 1 for the neutral clusters while the anions are shown in Fig. 2. Depending on the experimental conditions, more than one isomer and/or spin state can be produced in the beam.

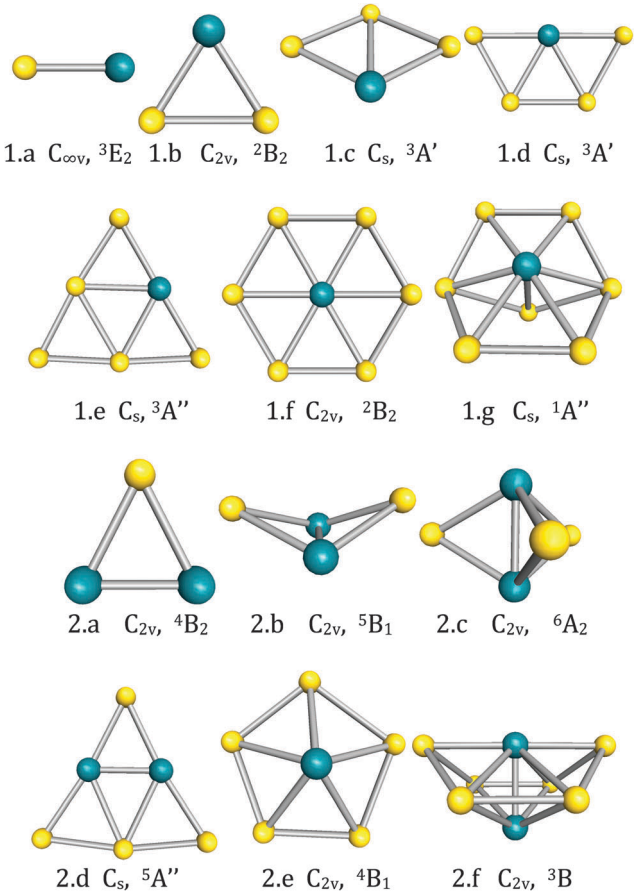

Fig. 1 Atomic Au_nRh_m neutral clusters for n = 1–7 and m = 1–2 atoms with their corresponding symmetry group and electronic state.

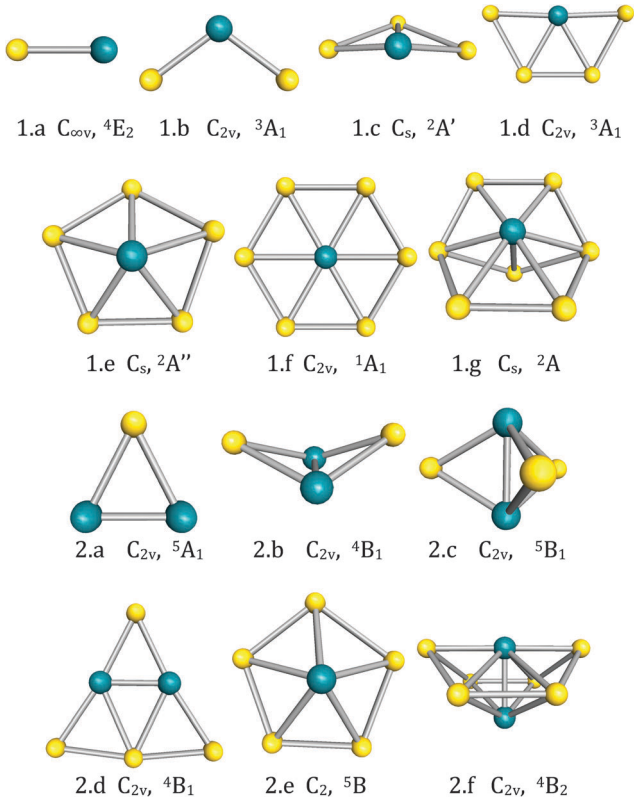

Fig. 2 Atomic Au_nRh_m anionic clusters for n = 1–7 and m = 1–2 atoms with their corresponding symmetry group and electronic state.

Therefore, for a synergistic interpretation of the PES spectra, the calculations must include all allowed spin states and all possible isomeric forms for both the neutral and charged configurations. As will be discussed further, if the calculated energies agree with experimental data, we consider that the ground state geometry and its multiplicity have been identified. In order to calibrate our methodology first of all we compare some of our results with previous theoretical calculations in ref. 8 and with the available experimental data,[43,44] such comparison can be seen in Table 1 for Au_2, Rh_2 and AuRh. When we only have gold, we have a bond length of 2.53 Å. This compares very well with the 2.47 Å experimental value and is very close to the calculated 2.54 Å in ref. 8. For rhodium we obtain 2.29 Å which is very similar to the experimental value of 2.28 Å also close to the theoretical calculation of 2.32 Å in ref. 8. Finally, for the AuRh mix we have calculated a bond length of 2.41 Å, and a vibrational frequency of 196 cm^{-1} for which no previous experimental data are available. Our result agrees well with the previously calculated value of 2.52 Å for the bond length and the frequency of 199 cm^{-1} in ref. 8. The calculated bond lengths have been used as an initial guess parameter in the symmetry unrestricted and unconstrained search for the lowest minima structures here presented. The Au–Au calculated binding energy compares well with the experimental data, and the fact that it is smaller than the Au–Rh binding energy suggests that the rhodium is going to prefer highly coordinated sites.

4 Results and discussion

4.1 Experimental results

The experimental results for the anion photoelectron spectra of $AuRh^-$, Au_2Rh^-, $AuRh_2^-$, $Au_2Rh_2^-$ have been recorded at 355 nm photon energy and are presented as a function of EBE in Fig. 3. The energy difference between the ground state of the anion and the ground state of its neutral is defined as the electron affinity (EA). Computationally the adiabatic detachment energy (ADE) which is defined as the energy difference between the ground state (GS) of the anion and the neutral relaxed to its nearest local minimum. If the neutrals nearest local minimum is also the global minimum, ADE and EA are actually the same values. The vertical transition between the anion ground state and the neutral cluster at the geometry of the anion (GA) is defined as the vertical detachment energy (VDE), and it corresponds to the first EBE peak in each spectrum. The VDE is the most reliable experimental value with which to compare with theory, they are calculated according to:

$$\mathrm{ADE} = E_{\mathrm{GS}}(\mathrm{Au}_n\mathrm{Rh}_m)^- - E_{\mathrm{GS}}(\mathrm{Au}_n\mathrm{Rh}_m)$$

$$\mathrm{VDE} = E_{\mathrm{GS}}(\mathrm{Au}_n\mathrm{Rh}_m)^- - E_{\mathrm{GA}}(\mathrm{Au}_n\mathrm{Rh}_m)$$

Experimentally the PES for $AuRh^-$, Au_2Rh^-, $AuRh_2^-$, $Au_2Rh_2^-$ have been obtained and are shown in Fig. 3. The PES recorded for $AuRh^-$ is shown in Fig. 3(a). The experimental EBE peak is at 1.40 eV which agrees reasonably well with the calculated value of 1.38 eV (see column 3 in Table 2). The experimental EA is located at about 1.31 eV, while our calculated value is 1.33, again very close to the experimental finding and suggesting that the structure corresponds to the dimer shown in Fig. 1(1.a) with symmetry group $C_{\infty v}$. Its electronic state corresponds to $^3E_2$. The second peak, located at 1.96 eV, is 0.56 eV after the first peak, which is in great agreement with the calculated H–L gap, 0.57 eV (see Table 3). The second experimental PES for Au_2Rh^- is that shown in Fig. 3(b) where it can been seen that the EBE peak is located at 3.33 eV. Our predicted VDE value is 3.34 eV, with a very good agreement with the experimental finding. Experimentally, the measured EA is located at 2.6 eV while the calculated one is found to be at 2.64 eV, again in good agreement. This confirms that it corresponds to the triangular structure shown in Fig. 1(1.b) with symmetry group C_{2v} and with an electronic state $^2B_2$. For the case of the $AuRh_2^-$ which is shown in Fig. 3(c) the EBE peak is located at 1.6 eV while our theoretical result is 1.57 as shown in column 3 in Table 2. The experimental ADE is 1.4 eV, while the calculated one is located at 1.5 eV. This confirms that it corresponds to the triangular structure shown in Fig. 1(2.a) which also has a symmetry group C_{2v} and an electronic state of $^4B_2$. There are more features on the high EBE end in Fig. 3(c), which are due to the transitions to higher states of the neutral. The last experimental PES spectrum is the one corresponding to $Au_2Rh_2^-$ and it is shown in Fig. 3(d). Even though it is noisy, we speculate that the EBE peak is located at 2.5 eV, and the theoretical prediction is found to be 2.47 eV, which is in good agreement. The EA corresponds to 2.1 eV and the theoretical

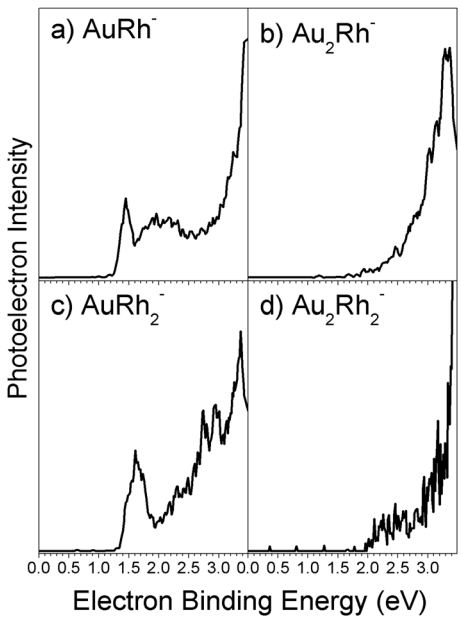

Fig. 3 Photo electron spectra for $Au_nRh_m^-$ clusters for n = 1–2 and m = 1–2 atoms.

Table 2 Calculated adiabatic detachment energies, vertical detachment energies, ionization potentials, binding energies per atom, first and second derivatives of the energy for Au_nRh_m (n = 1–7, m = 1–2) clusters, respectively. All units are given in eV

Cluster	ADE	VDE	IP	E_b/atom	ΔE	$\Delta^2 E$
AuRh	1.33	1.38	8.44	1.20	2.41	0.51
Au_2Rh	2.64	3.34	7.37	1.43	1.90	−1.37
Au_3Rh	2.18	2.35	7.70	1.68	2.41	0.33
Au_4Rh	2.55	2.76	7.13	1.76	2.08	−0.47
Au_5Rh	2.65	2.72	7.02	1.93	2.75	0.18
Au_6Rh	2.64	2.87	7.70	2.02	2.81	−0.84
Au_7Rh	2.91	3.08	7.08	2.01	1.84	
$AuRh_2$	1.52	1.57	7.00	1.86	2.31	−0.16
Au_2Rh_2	2.15	2.47	7.15	1.99	2.48	0.32
Au_3Rh_2	2.35	2.53	7.07	2.02	2.15	−0.53
Au_4Rh_2	2.54	2.59	7.59	2.13	2.68	0.46
Au_5Rh_2	2.78	2.99	7.10	2.14	2.21	−0.44
Au_6Rh_2	2.57	2.61	6.68	2.17	2.39	

Table 3 Cluster structure, multiplicity for both anionic and neutral clusters, HOMO–LUMO gaps and defragmentation energy (in electron volts) for Au_nRh_m (n = 1–7, m = 1, 2)

	$M = 2S + 1$		H–L (GAP)		D.E.	
Cluster	Anion	Neutral	Anion	Neutral	Rh	Au
AuRh	4	3	0.31	0.57	2.41	2.41
Au_2Rh	3	2	0.48	0.35	2.08	1.90
Au_3Rh	2	3	0.33	0.48	3.39	2.41
Au_4Rh	3	2	0.47	0.22	3.02	2.08
Au_5Rh	2	3	0.29	0.46	3.65	2.75
Au_6Rh	3	2	0.06	0.65	3.26	2.81
Au_7Rh	2	1	0.73	0.64	3.60	1.85
$AuRh_2$	5	4	0.26	0.27	3.07	2.31
Au_2Rh_2	4	5	0.21	0.45	3.65	2.48
Au_3Rh_2	5	6	0.27	0.73	3.40	2.15
Au_4Rh_2	4	5	0.27	0.38	4.00	2.68
Au_5Rh_2	5	4	0.37	0.31	3.43	2.21
Au_6Rh_2	4	3	0.21	0.23	3.22	2.39

prediction is 2.1 eV, (Table 2) confirming the bent rhombus structure shown in Fig. 1(2.b) with symmetry group C_{2v} and with the electronic state of $^5B_1$, we speculated that the second peak is located at 3.04 eV, 0.54 eV after the first peak, which is also in good agreement with the calculated H–L gap, 0.45 eV (see Table 3). For the clusters that could be confirmed experimentally we observe that the largest difference between the ADE and VDE is for the Au_2Rh cluster case where there is a marked geometry change from the anionic to the neutral ground state (see Fig. 1(1.b) for the neutral *versus* Fig. 2(1.b) for the anionic one). The calculated ADE and VDE values for the larger clusters corresponding to Au_nRh_m clusters (n = 3–7, m = 1–2) were only obtained by means of simulations. The procedure we followed for the theoretical assignment has been discussed at length in Section 3. All of our predicted VDE and ADE results are listed in columns 2 and 3 in Table 2. The ionization potential defined as the energy difference between the cationic state and the neutral is depicted in column 4 Table 2. This quantity is much larger in our clusters than that observed in the bulk phase. It is generally used as a parameter to measure the stability of a given species, therefore we can argue that the results here presented are plausible for mass production and therefore good candidates for future applications as the IP's reported are rather large.

4.2 Theoretical results

4.2.1 Au_nRh. The calculated ground state structures for Au_nRh_m (n = 1–7, m = 1, 2) for the neutral clusters are shown in Fig. 1, while the anions are shown in Fig. 2, both with their corresponding group symmetry and electronic states. The first thing to notice is that all neutral as well as charged clusters are planar for Au_nRh n = 1–6 with the exception of Au_7Rh which is 3-D but its corresponding planar structure is only 0.02 eV above. This result is different that the one obtained by Yang Ji-Xian *et al.* in ref. 8 who found a three dimensional ground state geometry for Au_5Rh. This same structure when subjected to our methodology is higher in energy by 0.16 eV with respect to our lowest (planar) structure which is depicted in Fig. 1(1.e). Finally we remark that this structure when negatively charged (anionic) is indeed non-planar (see Fig. 2(1.e)) agreeing well with the structure found in ref. 8. In general terms we found that the energy difference between planar and non-planar structures decreases as the number of gold atoms increases in the cluster. These (planar-(non-planar)) energy differences for the neutral clusters are shown graphically in Fig. 4. Another interesting finding is that the most stable cluster structures occur for the case when an even number of gold atoms is present and it is correlated with the fact that the atom positions are very specific. The rhodium atom always lies in a highly coordinated site, this can also be correlated with the considerable charge transfer towards the rhodium atom from its surrounding neighbors. This charge transfer tends to increase with the cluster size *i.e.* number of gold atoms. Graphically this can be seen in Fig. 5 for neutral clusters. An interesting point to notice is the parallelism between the well known planar characteristic of pure gold clusters for sizes 2–13 atoms *versus*

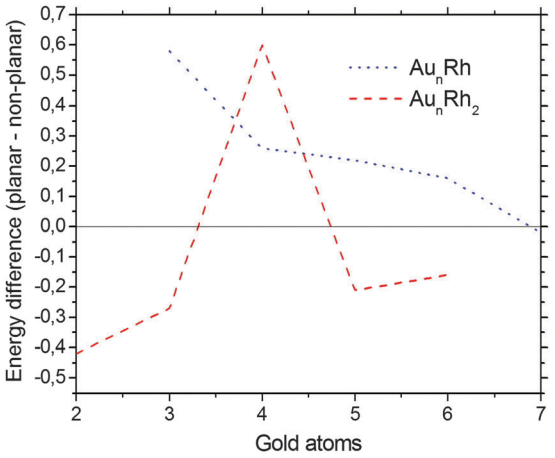

Fig. 4 Energy difference between the lowest planar and non-planar neutral Au_nRh_m cluster structures given in eV.

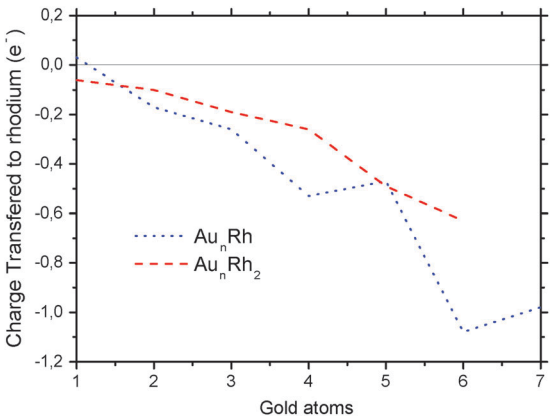

Fig. 5 Charge transfer calculated on neutral Au_nRh_m clusters towards the rhodium atoms according to the Mulliken approximation.

the geometries of the gold rhodium mix structures, for up to 7 atoms which are also planar. The planarity is broken for Au_7Rh, nevertheless its ((non-planar)-planar) energy difference is very small −0.02 eV (see Fig. 4). This energy is smaller than the k_BT thermal energy given by the room temperature, therefore it is expected to coexist. While its equivalent geometric structure (Au_8) has a much larger ((non-planar) –planar) energy difference of 0.1 eV per atom.[7] The arguments here exposed regarding their stability is supported by both, the analysis of the first and second derivative of the energy which have been calculated as:

$$\Delta E(Au_nRh_m) = E(Au_{n-1}Rh_m) + E(Au) - E(Au_nRh_m)$$

$$\Delta^2 E(Au_nRh_m) = 2E(Au_nRh_m) - E(Au_{n+1}Rh) - E(Au_{n-1}Rh_m).$$

Table 3 shows the multiplicity for the clusters here studied in columns 2 and 3. For clarity the trend of the magnetic moment is shown in Fig. 6, we found that it oscillates with the number of gold atoms in the mix being enhanced for even numbered in the case of the anionic clusters. The same result applies for the odd numbered clusters in the case of the neutral

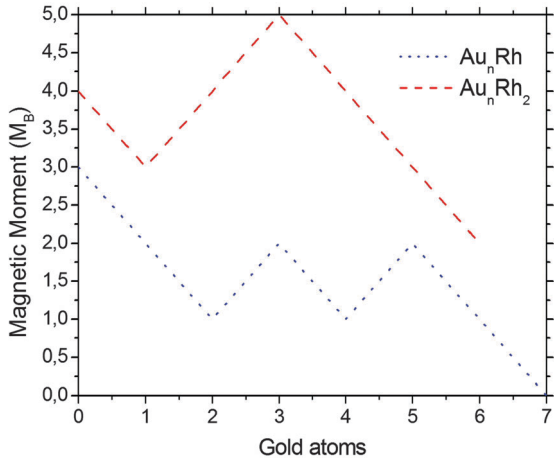

Fig. 6 Total magnetic moment as the number of gold atoms increases for Au_nRh_m neutral clusters.

clusters. The stability of the clusters increases for those who depict higher multiplicity, this correlates with larger gaps as can be seen in columns 4 and 5 in Table 3. We perform a study of the stability by means of the defragmentation energy which we calculate according to the following formulae:

$$Au_nRh_m + \Delta E \rightarrow Au_nRh_{m-1} + Rh$$

$$Au_nRh_m + \Delta E \rightarrow Au_{n-1}Rh_m + Au.$$

The defragmentation energy analysis shows that the energy required to dissociate one rhodium atom is larger than the necessary to dissociate a gold atom. We found that Au_5Rh is the most stable structure as the biggest defragmentation energy is required to remove the rhodium from this cluster. We remark that this structure is equivalent to the one proposed for Au_6. As a general trend we can observe in Table 3 that the defragmentation energy from the structures with an even number of atoms is more stable than that from the odd numbered ones. Finally, Fig. 7 and 8 show the Infra Red (IR) simulated spectra corresponding to the ground state neutral and anionic clusters corresponding to the structures shown in Fig. 1 and 2, respectively. The intensities of the bands in the IR spectra are normalized to the largest peak.

4.2.2 Au_nRh_2. The ground state structures for Au_nRh_2 (for n = 1–7) clusters are shown in Fig. 1(2.a–f) with their corresponding group symmetry and electronic state. The first thing to notice is that opposed to the case for the clusters containing only one rhodium atom which are planar, the structures with two rhodium atoms are all three dimensional, with the exception

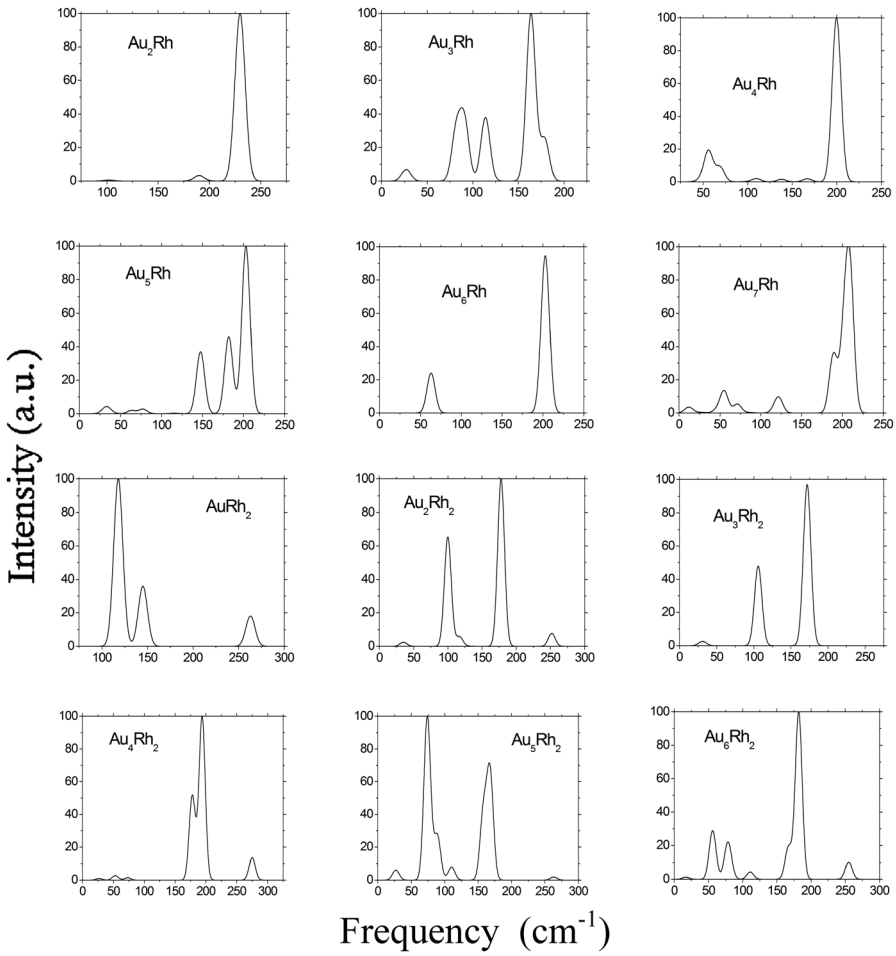

Fig. 7 Infra red spectra for Au_nRh_m (n = 1–7, m = 1, 2) neutral clusters in arbitrary units (the vertical axis is referred to the maximum peak intensity).

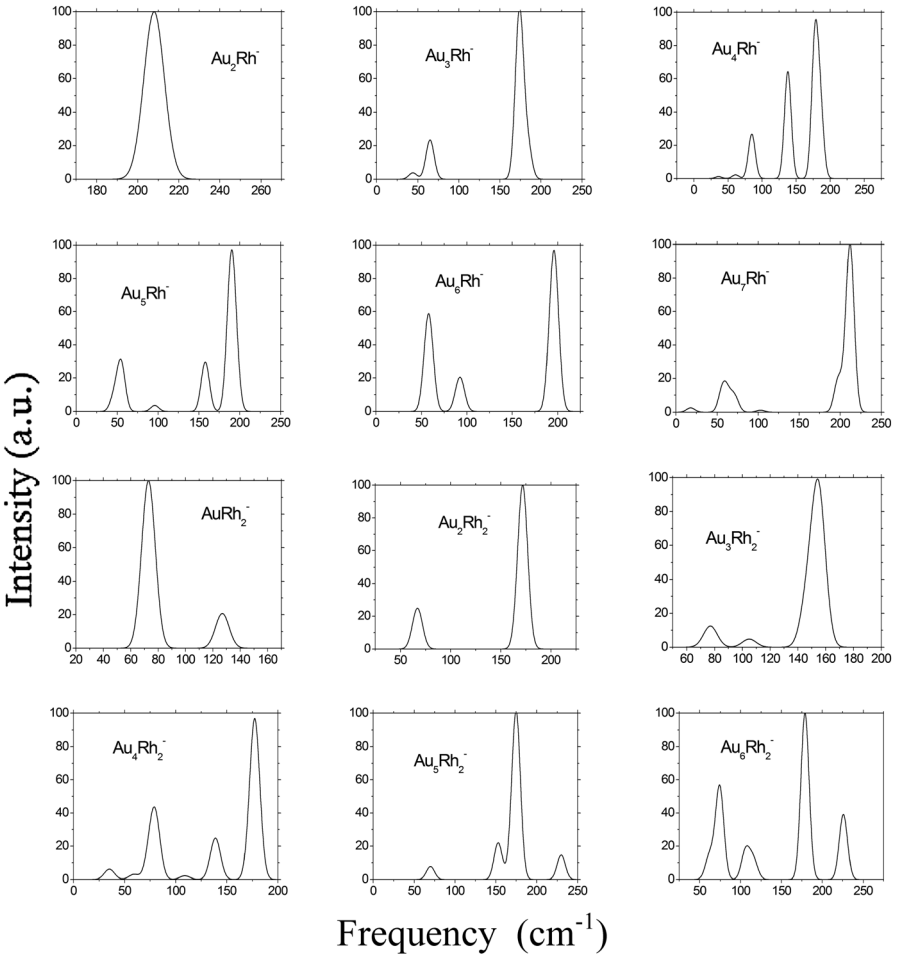

Fig. 8 Infra red spectra for Au_nRh_m (n = 1–7, m = 1, 2) anionic clusters in arbitrary units (the vertical axis is referred to the maximum peak intensity).

of Au_4Rh_2 shown in Fig. 1(2.d), which is very similar to the pure gold cluster with six atoms.[7] Nevertheless, despite being three dimensional one can see that the gold atoms tend to remain in one plane, while the rhodium atoms are displaced from it. Another thing we can remark is the fact that in the process of the cluster formation, rhodium binds preferably to another rhodium atom, this can be explained due to the difference in magnitude between Rh–Rh > Au–Rh > Au–Au binding energies. This can be seen clearly in the case of Au_3Rh_2 in Fig. 1(2.c) where the gold atoms do not bind amongst themselves but always to the rhodium atoms. And it also explains why all Au_nRh_2 structures have many group symmetry operations with respect to the axis formed between the two rhodium atoms, in particular they all have a mirror plane symmetry. Curiously enough the energy difference of the two rhodium atom clusters between the non-planar and planar structures decreases with the number of gold atoms (with the exception of Au_4Rh_2 where the non-planar structure is higher in energy). This is imprinted by the well known gold relativistic effects. With regard to their magnetic properties the addition of one rhodium atom contributes to their total magnetization with 2 μ_B. The magnetic behavior with the addition of gold atoms is similar to the one observed in the anionic clusters in the previous section for the Au_nRh clusters. However the magnetic moment for the neutral clusters oscillates in a bigger range of values and is consistent with the energy HOMO–LUMO difference as can be seen in Table 3. Table 3 also shows the defragmentation energy for all neutral clusters here investigated. One can notice that once more, that the dissociative energy for rhodium is larger than for gold, in all cases, this reinforces the idea that rhodium binds more strongly than gold, and explains why rhodium binds to itself and also why it always remains in the center of the clusters. We remark from Table 3 the fact that Au_4Rh_2 has the largest defragmentation energy and has also a structure similar to that of Au_6 and incidentally to Au_5Rh. This strange coincidence may be caused by the fact that they all have the same number of electrons in the last s-orbital. Their IR spectra is shown in Fig. 7 for the neutral clusters and Fig. 8 for the anions. Their peaks are constantly shifted to the left when we compare them with the IR's corresponding to the one rhodium atom case structures. This is due to the differences in mass and also the binding energy increase (see column 6 in Table 2) in the latter.

5 Conclusions

We have performed a comprehensive study of the energetic, structural, electronic, and magnetic properties of charged and neutral Au_nRh_m (m = 1–7, n = 1–2) clusters, by using a synergistic

approach which combined anion photoelectron spectroscopy and DFT based theoretical calculations. The total energy calculations quantitatively account for the photodetachment spectra and validates that the ground state structures and their magnetic moment have been univocally identified. ADE, VDE, binding energy, defragmentation energy, IR spectra, as well as the HOMO–LUMO gaps have also been calculated for these structures. The stability and dependence of these properties on the cluster sizes have been analyzed and discussed. We have found that Au_nRh are planar for up to 7 atoms while for Au_nRh_2 the structures are definitively not planar with the exception of Au_4R_2 which shows very similar characteristics to both Au_6 and Au_5Rh. Another striking result is the magnetic moment which seems to remain unaffected with the addition of gold atoms in the mix. We find that the structures are more stable when they contain an even number of atoms. This is a generalization of the result found earlier by Yang Ji-Xian *et al.* ref. 8. We have shown here how the combined use of an experimental technique (PES) and electronic structure theory can provide detailed information about the structures of binary clusters of gold and late transition metal clusters.

Acknowledgements

M.R.B. and F.B.Z. acknowledge the financial support from PAPIIT IN110112, and IN100515 UNAM project, and from DGSCA UNAM. Some calculations were performed at the supercomputer center in UNAM. F.B.Z. acknowledges support from CONACYT (financial support No. 227089), and to the IIM-UNAM (Instituto de Investigaciones en Materiales, Universidad Nacional Autónoma de México). This material is based in part on work supported by the (US) National Science Foundation under Grant No. CHE-1360692 (KHB).

References

1 H. Häkkinen and U. Landman, *Phys. Rev. B*, 2000, **62**, R2287.
2 M. R. Beltrán, F. Buendía, V. Chauhan, P. Sen, H. Wang, Y. J. Ko and L. Bowen, *European J. Phys. D.*, 2013, **67**, 63.
3 B. V. Reddy, S. N. Khanna and B. I. Dunlap, *Phys. Rev. Lett.*, 1993, **70**, 3323.
4 B. V. Reddy, S. K. Nayak, S. N. Khanna, B. K. Rao and P. Jena, *Phys. Rev. B*, 1999, **59**, 5214.
5 Y.-C. Bae, H. Osanai, V. Kumar and Y. Kawazoe, *Phys. Rev. B*, 2004, **70**, 195413.
6 M. Eichelbaum, K. Rademann, A. Hoell, D. M. Tatchev, W. Weigel, R. Stober and G. Pachioni, *Nanotechnology*, 2008, **19**, 135701.
7 L. Xao, B. Tollberg, X. Hu and L. Wang, *J. Chem. Phys.*, 2006, **124**, 114309.
8 Y. Ji-Xian, W. Cheng-Fuand and G. Jian-Jun, *Physica B*, 2010, **405**, 4892.
9 R. L. Chantry, I. Atanasov, S. L. Horswell, Z. Y. Li and R. L. Johnston, *Gold Clusters, Colloids and Nanoparticles, Structe and Bonding, 162, 162: 6790*, Springer International Publishing Switzerland, 2014.
10 D. Schooss, P. Weis, O. Hampe and M. M. Kappes, *Philos. Trans. R. Soc., A*, 2010, **368**, 1211.
11 L.-M. Wang and L.-S. Wang, *Nanoscale*, 2012, **4**, 4038.
12 P. Gruene, B. Butschke, H. T. Lyon, D. M. Rayner and A. Fielicke, *Z. Phys. Chem.*, 2014, 0480.
13 P. Gruene, D. M. Rayner, B. Redlich, A. F. G. van der Meer, J. T. Lyon, G. Meijer and A. Fielicke, *Science*, 2008, **321**, 674.
14 L. M. Ghiringhelli, P. Gruene, L. T. Lyon, D. M. Rayner, G. Meijer, A. Fielicke and M. Scheffler, *New J. Phys.*, 2013, **15**, 083003.
15 J. Jackschath, I. Rabin and W. Schulze, *Ber. Bunsenges. Phys. Chem.*, 1992, **96**, 1200.
16 G. Bravo-Pérez, I. L. Garzón and O. Novaro, *THEOCHEM*, 1999, **493**, 225.
17 H. Grönbeck and W. Andreoni, *Chem. Phys.*, 2000, **262**, 1.
18 V. Bonacic-Koutecký, J. Burda, R. Mitric, M. Ge, G. Zampella and P. Fantucci, *J. Chem. Phys.*, 2002, **117**, 3120.
19 E. M. Fernandez, J. M. Soler, I. L. Garzón and L. C. Balbás, *Phys. Rev. B*, 2004, **70**, 165403.
20 F. Remacle and E. S. Kryachko, *J. Chem. Phys.*, 2005, **122**, 044304.
21 B. Assadollahzadeth and P. Schwerdtfeger, *J. Chem. Phys.*, 2009, **131**, 064306.
22 H. M. Lee and K. S. Kim, *Chem. – Eur. J.*, 2012, **18**, 13203.
23 D. A. Götz, R. Schäfer and P. Schwerdtfeger, *J. Comput. Chem.*, 2013, **34**, 1975.
24 J. Wang, G. Wang and J. Zhao, *Phys. Rev. B: Condens. Matter Mater. Phys.*, 2002, **66**, 035418.
25 R. M. Olson, S. Varganov, M. S. Gordon, H. Metiu, S. Chretien, P. Piecuch, K. Kowalski, S. A. Kucharski and M. Musial, *J. Am. Chem. Soc.*, 2005, **127**, 1049.
26 P. Ghosh, R. Pushpa, S. de Gironcoli and S. Narasimhan, *J. Chem. Phys.*, 2008, **128**, 194708.
27 S. M. Hamilton, W. S. Hopkins, D. J. Harding, T. R. Walsh, P. Gruene, M. Haertelt, A. Fielicke, G. Meijer and S. Mackenzie, *J. Am. Chem. Soc.*, 2010, **132**, 1448.
28 S. M. Hamilton, W. S. Hopkins, D. J. Harding, T. R. Walsh, M. Haertelt, C. Kerpal, P. Gruene, G. Meijer, A. Fielicke and S. Mackenzie, *J. Phys. Chem. A*, 2011, **115**, 2489; A. Fielicke, G. von Helden, G. Meijer, D. B. Pedersen, B. Simard and D. M. Rayner, *J. Phys. Chem. B*, 2004, **108**, 14591.
29 A. Fielicke, P. Gruene, G. Mejier and D. M. Rayner, *Surf. Sci.*, 2009, **603**, 1427.
30 X. Li, A. Grubisic, S. T. Stokes, J. Cordes, G. F. Gantefoer, K. H. Bowen, B. Kiran, M. Willis, P. Jena, R. Burgert and H. Schnoeckel, *Science*, 2007, **315**, 356.
31 H. Wang, Y. J. Ko, L. G. García, P. Sen, M. R. Beltrán and K. H. Bowen, *Phys. Chem. Chem. Phys.*, 2011, **13**, 7685.
32 D. J. Harding, T. R. Walsh, S. M. Hamilton, W. S. Hopkins, S. R. Mackenzie, P. Gruene, M. Haertelt, G. Meijer and A. Fielicke, *J. Chem. Phys.*, 2010, **132**, 011101.
33 D. J. Harding, P. Gruene, M. Haertelt, G. Meijer, A. Fielicke, S. M. Hamilton, W. S. Hopkins, S. R. Mackenzie, S. P. Neville and T. R. Walsh, *J. Chem. Phys.*, 2010, **133**, 214304.

34 A. J. Cox, J. G. Louderback and L. A. Bloomfield, *Phys. Rev. Lett.*, 1993, **71**, 923.
35 A. J. Cox, J. G. Louderback, S. E. Apsel and L. A. Bloomfield, *Phys. Rev. B*, 1994, **49**, 12295.
36 M. Gerhards, O. C. Thomas, J. M. Nilles, W. J. Zheng and K. H. Bowen, *J. Chem. Phys.*, 2002, **116**, 10247.
37 D. G. Leopold, J. Ho and W. C. Lineberger, *J. Chem. Phys.*, 1987, **86**, 1715.
38 R. Ahlrichs, M. Bar, M. Haser, H. Horn and C. Kolmel, *Chem. Phys. Lett.*, 1989, **162**, 165.
39 F. Weigend and R. Ahlrichs, *Phys. Chem. Chem. Phys.*, 2005, **7**, 3297.
40 J. P. Perdew, K. Burke and M. Ernzerhof, *Phys. Rev. Lett.*, 1996, **77**, 3865.
41 M. P. Johansson, A. Lechtken, D. Schoos, M. M. Kappes and F. Furche, *Phys. Rev. A*, 2008, **77**, 053202.
42 M. Mantina, R. Valero and D. G. Truhlar, *J. Chem. Phys.*, 2009, **131**, 064706.
43 K. A. Gingerich and D. L. Cocke, *J. Chem. Soc., Chem. Commun.*, 1972, **1**, 536.
44 K. P. Huber and G. Herzberg, *Molecular Spectra and Molecular structure IV. Constants of Diatomic Molecules*, Van Nostrand Reinhold Company, New York, 1979, p. 198.